Article:
Ozsoy, M. orcid.org/0000-0002-3069-7377, Sims, N.D. orcid.org/0000-0002-6292-6736 and Ozturk, E. (2022) Robotically assisted active vibration control in milling: a feasibility study. Mechanical Systems and Signal Processing, 177. 109152. ISSN 0888-3270

https://doi.org/10.1016/j.ymssp.2022.109152

Mechanical Systems and Signal Processing 177 (2022) 109152

Contents lists available at ScienceDirect

Mechanical Systems and Signal Processing

journal homepage: www.elsevier.com/locate/ymssp

Robotically assisted active vibration control in milling: A feasibility study

Muhammet Ozsoy [a,*], Neil D. Sims [a], Erdem Ozturk [b]

[a] Department of Mechanical Engineering, The University of Sheffield, Mappin Street Sheffield S1 3JD, UK
[b] Advanced Manufacturing Research Center with Boeing, The University of Sheffield, Wallis Way, Rotherham, Sheffield S60 5TZ, UK

ARTICLE INFO

Communicated by J.E. Mottershead

Keywords:
Robotic assisted milling
Active chatter control
Saturation sensitivity
Chatter stability
Inertial actuator

ABSTRACT

The role of robots has been increasing in machining applications, with new concepts such as robotic-assisted machining where a robot supports the workpiece while it is machined by a machine tool. This method improves chatter stability to a certain extent. However, forced vibrations or unstable vibrations such as chatter can still be a limiting factor for the productivity and quality of the machining process. In this paper, the robotically assisted milling approach is extended to consider an actively controlled robot arm, to suppress the chatter vibrations for milling operation. To assess the feasibility of the method, a proof-mass actuator is assembled on a beam structure that is representative of the robot system. The beam structure is designed to exhibit two degrees of freedom in its structural dynamics, thereby emulating the robots' dynamic response. The effect of active control is evaluated. Frequency domain results show that the actively controlled robot arm increases the chatter stability and critical limiting depth of cut. A range of active control methods are evaluated, namely direct velocity feedback (DVF), virtual passive absorber (VPA), proportional integrated derivative (PID), linear quadratic regulator (LQR), H infinity (H_∞) and μ synthesis control. To validate the simulated frequency response function (FRF) results, several experimental tests are carried out for each control method. Furthermore, a time domain model is used to validate the stability lobe diagrams by detecting the chatter boundaries with/without actuator force saturation. It is shown that the critical limiting depth of cut can be increased by a factor of 2.6, compared to the scenario where the robot has no active control applied.

1. Introduction

Regenerative chatter is the primary obstacle in machining processes. This form of machining chatter is a self-excited vibration that results in high cutting forces, poor surface quality and accelerated tool wear [1].

The phenomenon can especially affect the thin-walled and flexible structures due to their low dynamic stiffness. To avoid chatter, different modelling methods [2–4] can be used considering the dynamic response of the thin walled structure. For instance, Bravo et al. [3] presented a method for prediction of stability lobe diagram (SLD) by updating Altintas's method [5,6]. They developed a 3-dimensional SLD based on relative motion of the machine tool and flexible workpiece, however, the computational time is longer. The prediction method has been validated by milling experiments. Campa et al. [4] studied bull-nose end mills to avoid chatter in the milling of thin floors. They proposed an averaging method based on tool-path discretisation, prediction of modal parameters by finite element method (FEM) and the SLD representation. Several cutting trials were conducted to validate the method. They

* Corresponding author.
E-mail address: mozsoy1@sheffield.ac.uk (M. Ozsoy).

https://doi.org/10.1016/j.ymssp.2022.109152
Received 30 November 2021; Received in revised form 9 March 2022; Accepted 8 April 2022
Available online 30 April 2022

concluded that selecting the stable spindle speed can be difficult due to the variation of modal parameters which may result in uncertainty of SLD. In order to suppress the chatter, newly developed milling tools [7,8] can also be employed. Urbikain et al. [7] proposed a time-domain method using a barrel type, curved end mill tool to improve the chatter stability. Considering the runout and complex tool geometry, the prediction model was validated experimentally in flexible structure milling. Besides, taking into account the accelerometer mass effect can be a solution to improve the SLD prediction in thin-wall component milling. Olvera et al. [9] presented the effect of the accelerometer mass effect for the thin-walled structure. They compared the frequency response function (FRF) using an accelerometer and a noncontact laser Doppler vibrometer (LDV) system. SLDs were estimated by using the FRFs measured both accelerometer and LDV. It is concluded that the mass of the accelerometer results in SLD boundary deviation.

Additional damping, and other forms of structural modification, can also increase the regenerative chatter stability of a machining scenario. A passive tuned mass damper [10,11] is one possible solution, but this approach often requires manual intervention within the production process, and is unable to adapt its configuration based upon changes in the system's configuration. The latter aspect can be overcome by an active damping system [12].

In recent years, researchers [13,14] have proposed active control to suppress the chatter by using an inertial actuator. Direct velocity feedback (DVF) has been extensively considered [15–17] since it is easy to implement. However, it can be influenced by high frequency forces, necessitating a filter within the implementation electronics. Model based control methods such as the linear quadratic regulator or H infinity control can be implemented to improve the chatter stability [18,19]. However, to conduct these control methods, the dynamic response of the structure must be known to tune the control parameters [20]. Using μ synthesis as an active control method in machining has some benefits [21–23]. First, the controller can be designed to guarantee the stability in terms of chatter. Second, the robust machining stability performance can be achieved regarding the actuator, machine tool or the support structure uncertainties. In general, despite this previous research, active damping systems face practical problems when used for chatter mitigation, due to the need for installation and configuration of the device within a production environment.

Robotic machining has been proposed recently because it offers advantages such as large reorientation capability, low cost, and greater versatility. Verl et al. [24] presented recent work focusing on milling, turning, drilling, grinding and polishing. Although the productivity is increased, there are still some challenges such as tool path accuracy, process control, and kinematics programming to be overcome.

A more pragmatic approach is so-called robotic assisted machining [25–27], where robotic devices are used to increase productivity without being part of the main material removal subsystem. For instance, as a mobile support application, Ozturk et al. [28] used a robot to support the workpiece whilst the robot moves together with the cutting tool. Experimental results showed that the form error decreased by implementing a moving support. However, only static form errors could be considered by the approach, rather than the dynamic motion associated with regenerative chatter.

In this research paper, a mobile active vibration control method using a robot arm is proposed for milling operations. This seeks to overcome the disadvantages of active vibration control methods by harnessing the automation capabilities of robotically assisted approaches. The aim is to demonstrate the feasibility of the approach and to compare the performance of different vibration control strategies. The remainder of the paper is organised as follows. First, the problem being considered is illustrated in more detail, and a simplified dynamics scenario is defined. Time-domain and frequency-domain models of the system are introduced as these will form the basis of the numerical study. Then, several candidate control systems are designed and the chatter stability is predicted for each scenario. Simulation results are then validated against experimental vibration tests. The discussion section follows to explain the performance differences between control methods; finally, conclusions are drawn.

2. Machining configuration

This section describes the ultimate objective of the robotically assisted chatter suppression method and then proposes a simplified numerical scenario that is used as a feasibility study.

2.1. Robotically assisted active vibration control

The concept of robotically assisted active vibration control in milling is illustrated schematically in Fig. 1. Here, a six-axis industrial robot is used to position an end effector against the machining workpiece. The workpiece is otherwise clamped in position using traditional workpiece fixturing techniques. The robot is articulated to achieve positive contact pressure between the end effector and the workpiece, in a similar fashion to previous work [28]. However, unlike previous work the end effector's main purpose is to impose dynamic forces upon the workpiece structure, by way of a proof-mass (or inertial) actuator, in order to increase the chatter stability during machining. The forces acting at the interface between the robot, workpiece, and tool are depicted in Fig. 1b. It can be seen that the proof-mass actuator force f_{act} will influence the total support force f_t, but it should be noted that this total support force can only be positive as the robot is not rigidly attached to the workpiece by the robot–workpiece interface. However, this support force will also be influenced by the forces transmitted through the robot structure itself. Consequently, the structural dynamics of the robot, and of the workpiece, need to be considered in order to design the control system for the inertial actuator.

The objective of the present contribution is to explore solutions to this design problem and assess the potential performance improvements, in terms of increased chatter stability. From a practical perspective, this solution would enable increased productivity from the machining operation, because greater material removal rates could be achieved without causing chatter. Meanwhile, the active controller and its robotic mount could be readily configured to re-deploy the active device, either at different locations on the workpiece (e.g. as the machining location is moved), or on different workpiece/machining configurations.

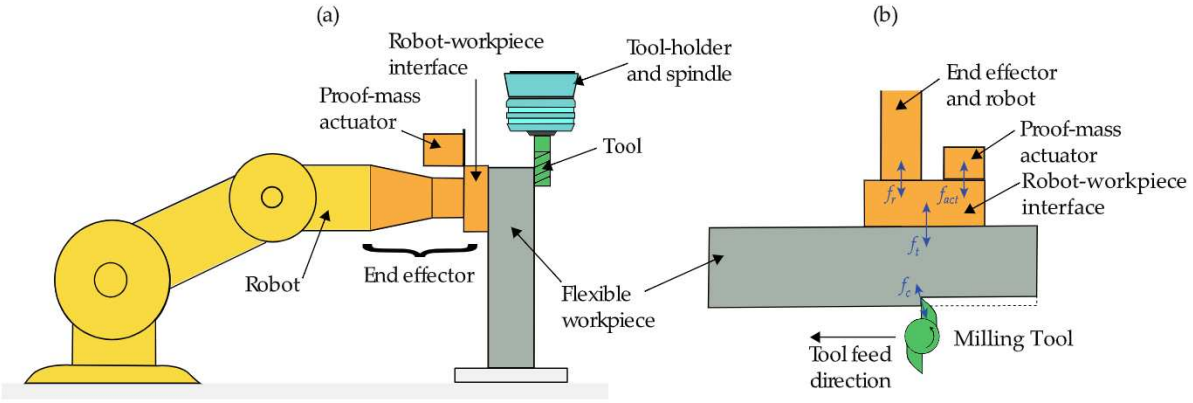

Fig. 1. Conceptual illustration of robotic assisted vibration control during milling. (a) side view; (b) top view, showing the cutting force f_c, total support force f_t, total proof-mass actuator force f_{act} and robot support force f_r.

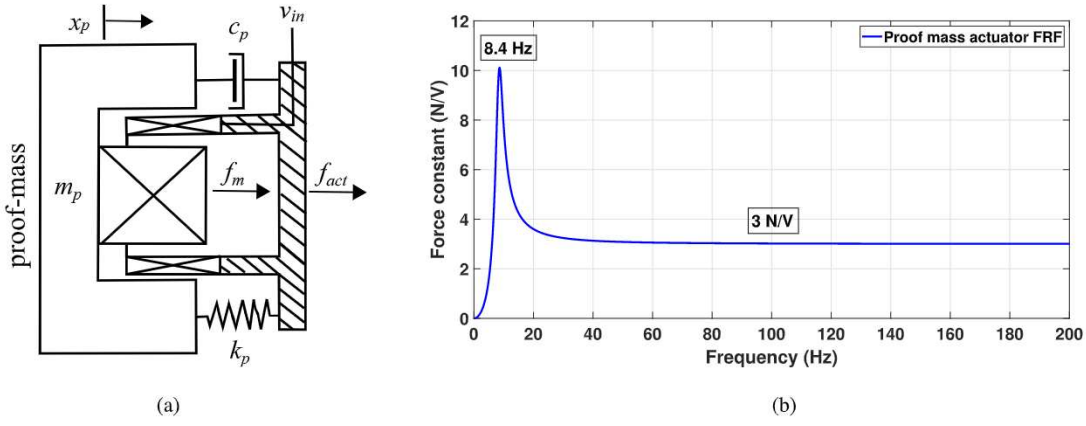

Fig. 2. (a) Proof-mass actuator; (b) Frequency response function [29].

2.2. Robot and actuator specification

In order to assess the feasibility of the proposed approach, representative models of the robot arm and the inertial actuator are required. For the present study, the model of the robot arm is motivated by the STAUBLI TX-90 industrial serial arm robot. Meanwhile, to simulate the effect of active vibration control, an inertial actuator specification and dynamic model is required. It should be noted that an inertial actuator is chosen as this approach is easily deployed on the robot's end effector: the actuator can achieve significant dynamic force control of the workpiece, but without changing the static force supplied by the robot manipulator, and without requiring direct rigid connection to an inertial reference frame (i.e. the ground).

A schematic illustration of an inertial actuator model is shown in Fig. 2(a).

The actuator is modelled by a moving mass m_p with a damper c_p and spring k_p. The mass is excited by an electromagnetic force f_m pursuant to the voltage input v_{in}. The resulting force on the host structure is f_{act}. The transfer function between the mass displacement x_p and the voltage input v_{in} can be written as,

$$\frac{X_p(s)}{V_{in}(s)} = \frac{G_1 G_2}{m_p s^2 + c_p s + k_p} \tag{1}$$

where V_{in} is the Laplace transform of v_{in}, X_p is the Laplace transform of x_p, G_1 is the electromagnetic gain and G_2 is the power amplifier gain [30]. The transfer function between the reaction force f_{act} and the voltage input v_{in} can be written as,

$$\frac{f_{act}(s)}{V_{in}(s)} = \frac{-G_1 G_2 m_p s^2}{m_p s^2 + c_p s + k_p} = g_a \frac{s^2}{s^2 + 2\zeta\omega_p s + \omega_p^2} \tag{2}$$

where ω_p is the natural frequency, ζ is the damping ratio of the actuator and $g_a = G_1 G_2$ is the actuator gain [30].

In the present study, the parameters for the actuator are based upon the ADD-45 inertial actuator from Micromega Dynamics [29]. This actuator has a mode at 8.4 Hz and is capable of applying up to 27 N supporting force up to 2000 Hz. The frequency response

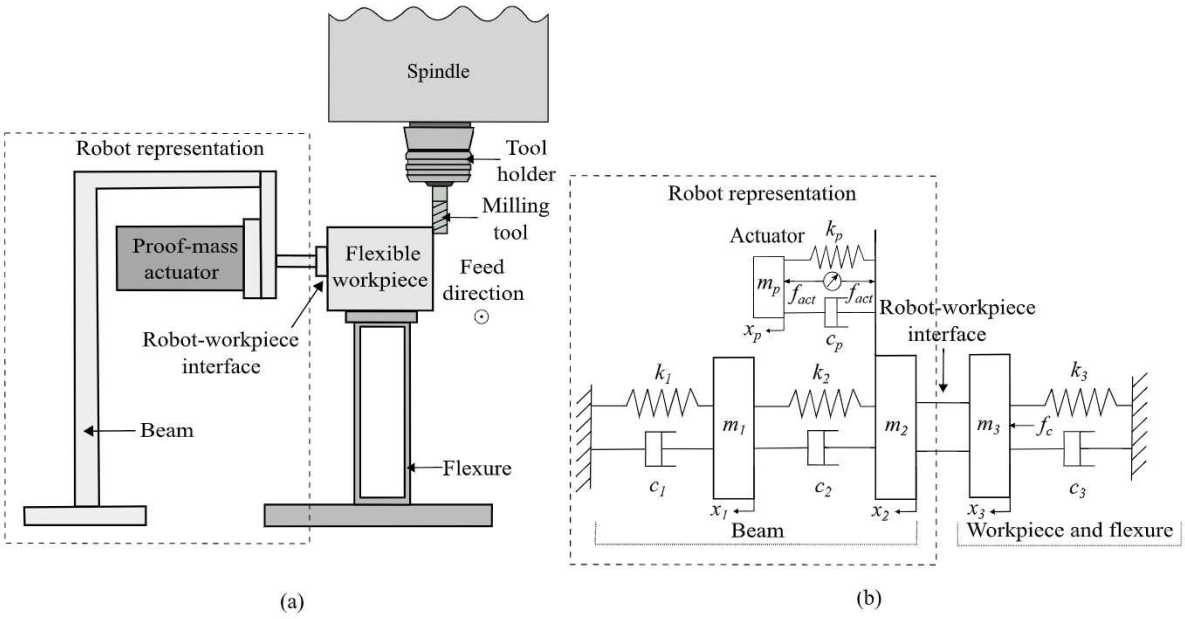

Fig. 3. Simplified model of the active vibration problem. (a) Schematic diagram; (b) Lumped parameter representation.

Table 1
Structural parameters.

Preloaded structural parameters	
Natural frequency	142.1 Hz
Damping ratio	0.88%
Stiffness	2.43×10^7 N m^{-1}
Flexible robot parameters	
Natural frequency	23 Hz, 47 Hz
Damping ratio	4.3%, 2.9%
Stiffness	7.9×10^5 N m^{-1}, 2×10^6 N m^{-1}

function (FRF) of the actuator can be seen in Fig. 2(b). The actuator transfer function can be written as:

$$\frac{f_{act}(s)}{V_{in}(s)} = 3\frac{s^2}{s^2 + 15.834s + 2785.6} \tag{3}$$

2.3. Simplified model

This subsection describes a numerical model of the active vibration control problem, for the purposes of control system design and performance/feasibility evaluation. The model parameters are based upon the properties of the physical systems described in Section 2.2. The model configuration is shown schematically in Fig. 3. Here, a two degree of freedom beam structure which emulates the flexible robot is pushed against a flexible workpiece. The beam structure is designed considering the most flexible modes of the Staubli robot, which were previously identified [31] as 23 Hz and 47 Hz. The robot and structure parameters which are given in Table 1, were identified by a tap testing. The workpiece in Fig. 3 is represented by a solid workpiece block that is mounted on a flexure, with natural frequency, damping ratio and stiffness values of 142.1 Hz, 0.88% and 2.43×10^7 N m^{-1}, respectively. The robot–workpiece interface is assumed to be a rigid contact, and it should be reiterated that the robot is not firmly attached at this location: with reference to Fig. 3, the contact force can only act to oppose the relative motion $x_3 - x_2$. In this way, future work can explore the experimental performance of the representative system, prior to deployment on a physical robotic/machining system that exhibits a higher number of modes of vibration.

The equation of motion for the structure is:

$$(m_2 + m_3)\ddot{x}_2 = -c_2(\dot{x}_2 - \dot{x}_1) - c_3\dot{x}_2 - c_p(\dot{x}_2 - \dot{x}_p) - k_2(x_2 - x_1) - k_3x_2 - k_p(x_2 - x_p) + f_c - f_{act} \tag{4}$$

3. Proposed control systems

The inertial actuator could implement any number of active vibration control schemes. Whilst there have been a large number of active vibration controllers considered for milling chatter mitigation [19,32,33], the specific scenario being considered here has not

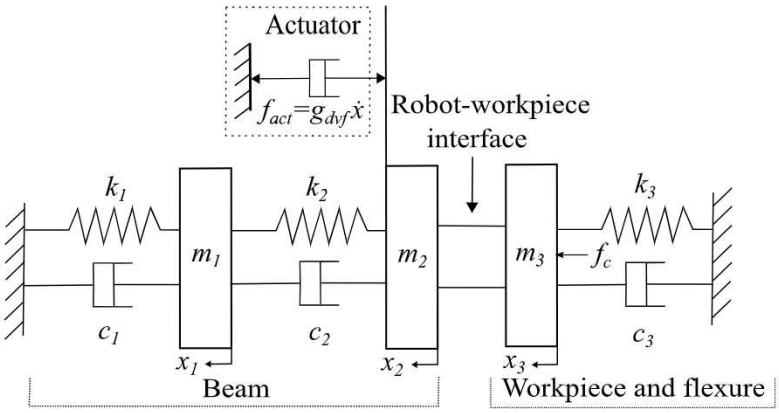

Fig. 4. Direct velocity feedback (DVF) control. The dashed box depicts the desired behaviour of the proof-mass actuator.

been previously explored. Consequently, one aim of the present work is to assess whether different controller designs offer better potential for the reduction of chatter, for example due to the impact of actuator saturation effects. Therefore, a range of candidate controller designs are considered, namely: direct velocity feedback (DVF), virtual passive absorber (VPA), proportional integrated derivative (PID), linear quadratic regulator (LQR), H-infinity (H_∞) and μ synthesis control.

However, each of these controllers requires the judicious choice of controller gains. In practice this tuning problem involves a compromise whereby more aggressive tuning parameters may lead to actuator saturation effects. In the present the controllers are tuned using an iterative optimisation method known as self adaptive differential evolution (SADE). This method is not in the scope of this paper, but the theory and method are addressed elsewhere [34]. The objective is to seek the value of the gain(s) where stability is maximised but actuator saturation does not occur. This is explained in detail in Section 4.1. First, for completeness, the different control strategies are briefly introduced.

3.1. DVF (Direct velocity feedback)

Direct velocity feedback (DVF) acts as a viscous damper by implementing an actuator force proportional to the structure's velocity. The velocity of the vibration is required as a feedback signal; this is typically obtained by integrating an acceleration measurement. This concept is depicted schematically in Fig. 4. The approach has been widely proposed by researcher [33,35,36] due to its simplicity. However, optimisation is required to find the optimal value of feedback gain.

If the active control force is provided by an inertial actuator, the closed-loop characteristic equation of the system with the actuator dynamics can be written as,

$$1 + g_{dvf}\, s \frac{g_a s^2}{s^2 + 2\zeta\omega_p s + \omega_p^2} G(s) = 0 \tag{5}$$

where ω_p, ζ, g_a, g_{dvf}, $G(s)$ are the natural frequency and damping ratio of the actuator, actuator gain, feedback gain and the system's transfer function, respectively [30].

3.2. VPA (Virtual passive absorber)

The Virtual Passive Absorber (VPA) control approach is depicted schematically in Fig. 5. The approach only requires modal properties of the structure to be controlled, in order to choose the control system parameters (natural frequency and damping ratio). The parameters can then be calculated using classical passive vibration absorber design strategies [37,38]. It has been shown that the VPA control method can be used to suppress the chatter vibrations successfully [33]. In the present paper, the tuning method proposed by Sims [11] is used. This algorithm, like many absorber optimisation algorithms, assumes a single mode of vibration. Consequently, the controller performance may be degraded if the dynamic properties of the structure change dramatically or if multiple modes of vibration are relevant to the chatter stability.

The closed-loop characteristic equation with VPA control can be described as [33],

$$1 + \frac{g_a s^2}{s^2 + 2\zeta\omega_p s + \omega_p^2} \frac{M\mu_c s^2 (2\zeta_a \omega_a s + \omega_a^2)}{g_a (s^2 + 2\zeta_a \omega_a s + \omega_a^2)} G(s) = 0 \tag{6}$$

Here, μ_c, ζ_a, ω_a are the mass ratio, the damping ratio and the natural frequency of the absorber, respectively. M is mass of the main structure. To compensate the actuator gain g_a, the control dynamic is multiplied by g_a^{-1}. The optimum passive absorber parameters (natural frequency and damping ratio) can be calculated as [11],

$$\frac{\omega_a}{\omega_n} = \sqrt{\frac{1}{1+\mu_c}} \qquad \zeta_a = \sqrt{\frac{3\mu_c}{8(1+\mu_c)}} \tag{7}$$

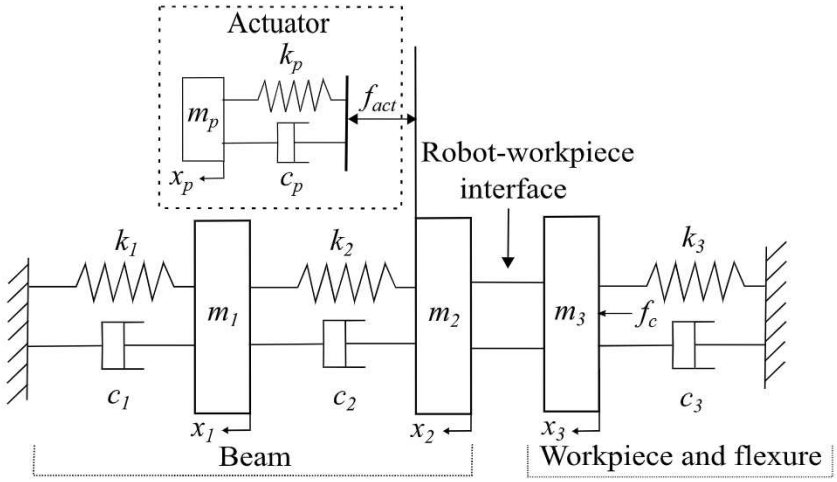

Fig. 5. Virtual passive absorber (VPA) control. The dashed box depicts the desired behaviour of the proof-mass actuator.

where, ω_n is the natural frequency of the main structure. The mass ratio μ_c is optimised with the SADE algorithm as described in Section 4.1.

3.3. PID (Proportional–integral–derivative)

Proportional integral and derivative (PID) control is well established [39], and its application to suppress chatter is reasonably promising [40–42]. The closed-loop characteristic equation with PID control can be written as,

$$1 + (g_{pp} + g_{pv}s + g_{pa}s^2)\frac{g_a s^2}{s^2 + 2\zeta\omega_p s + \omega_p^2}G(s) = 0 \tag{8}$$

where g_{pp}, g_{pv}, g_{pa} are the proportional, integral, derivative control gains, respectively, and are tuned using the SADE algorithm as described in Section 4.1.

3.4. LQR (Linear quadratic regulator)

A Linear quadratic regulator (LQR) is an optimal feedback controller that minimises a quadratic performance index, the takes into consideration the control input and the states. Two weighting matrices [30] must be chosen. The control method has been successfully applied to improve chatter stability [18,20].

Consider a state-variable system

$$\dot{x} = Ax + Bu \tag{9}$$

where the A and B are the state space representation of the system. The LQR is a state space control method, which means that the feedback is obtained by multiplying the state vector $x(t)$ with a matrix K [30]:

$$u(t) = -Kx(t). \tag{10}$$

To choose K, the cost function which needs to be minimised can be stated as:

$$J = \frac{1}{2}\int_0^\infty (x^T Qx + u^T Ru)dt \tag{11}$$

where Q is a positive semi-definite weighted matrix related to the state cost and R is a positive definite weighted matrix related to the control cost. The parameters Q and R are tuned numerically using the SADE algorithm in the present study. The state feedback gain matrix can then obtained:

$$K = R^{-1}B^T P \tag{12}$$

where P is the symmetric positive definite solution of the algebraic Riccati equation:

$$PA + A^T P + Q - PBR^{-1}B^T P = 0. \tag{13}$$

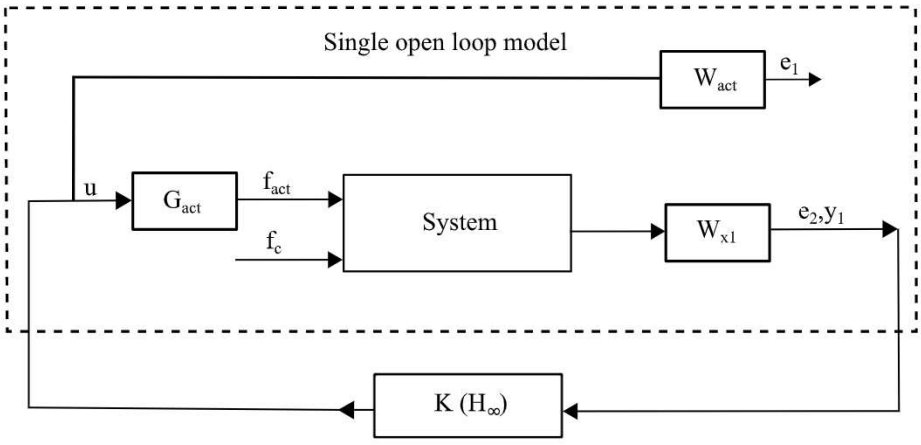

Fig. 6. H_∞ control method.

3.5. H_∞ (*H-infinity*)

In H_∞ control, weighting matrices are added to the feedback loop of the structural model and the controller, in order to improve performance and controller stability [43]. Recently, there have been significant efforts to apply H_∞ control method in machining dynamics problems [19,22,44,45]. The approach is summarised in Fig. 6. Here, W_{act}, is the actuator weighting function, W_{x1} is a weighting function to penalised the measured structural vibration, and G_{act} is the actuator transfer function described in the previous section. Single open loop model represents the generalised plant including the weighting functions, external disturbance (cutting force f_c) and the error signals e_1 and e_2 which need to be minimised to fulfil the control targets.

The actuator weighting function can be configured as a high pass filter to stabilise the actuator force in a specific bandwidth:

$$W_{act} = \frac{s^2}{s^2 + 2\zeta w_{hp} + \omega_{hp}^2} \tag{14}$$

where ω_{hp} is $2\pi \times 10$ rad/s; slightly above the natural frequency of the actuator (8.4 Hz).

To penalise the structural vibration, the weighting matrix W_{x1} can be stated as [46]:

$$W_{x1} = G_{st} \frac{\frac{s}{2\pi f_1} + 1}{\frac{s}{2\pi f_2} + 1} \tag{15}$$

where G_{st}, f_1, f_2 are the control parameters to be tuned using the SADE algorithm.

3.6. μ-*synthesis control*

A control system is robust if it is not sensitive to the differences between the model and the real system. These differences are referred to as uncertainties [43], and they can arise due to issues such as sensor failure, system parameter variations, and actuator dynamics. The control strategies introduced so far do not take into account these uncertainties, and yet such uncertainties are known to have a detrimental effect on chatter control [47–49].

The, μ synthesis control strategy can address this issue. The approach has been successfully applied by researchers [21–23] to obtain chatter free milling processes. In the context of the present study, μ synthesis control could help to avoid issues due to the changing dynamics of the robot, if it is reconfigured or repositioned during the machining operation. Similarly, the strategy could alleviate problems due to changing dynamics of the workpiece as material is removed. The μ synthesis control strategy is shown schematically in Fig. 7. Here, Δ_{act} and Δ_{sys} represent the uncertainties for the actuator and the main system, respectively.

The singular value of μ is a tool for the robust performance analysis with a given controller [43]. The μ synthesis problem is to seek a controller which reduces the μ condition iteratively. To find the optimal controller, The $D-K$ iteration approach [50,51] can be used to combine the H_∞ and μ analysis approach. This iterative method solves a convex optimisation problem. However, the D-K iteration approach can only consider the robustness of the system to dynamic uncertainties in the actuator, Δ_{act}. Consequently, the approach can be extended to mixed uncertainty cases. Here, the $D,G-K$ iteration procedure [52] obtains robust performance taking into account real and dynamic uncertainties Δ_{act} and Δ_{sys}. The iteration approach in general results in a high-order controller. Hence, the controller reduction can be applied to implement the proposed controller in practice. In the present study, the Hankel model [53] is used to reduce the order of the controller.

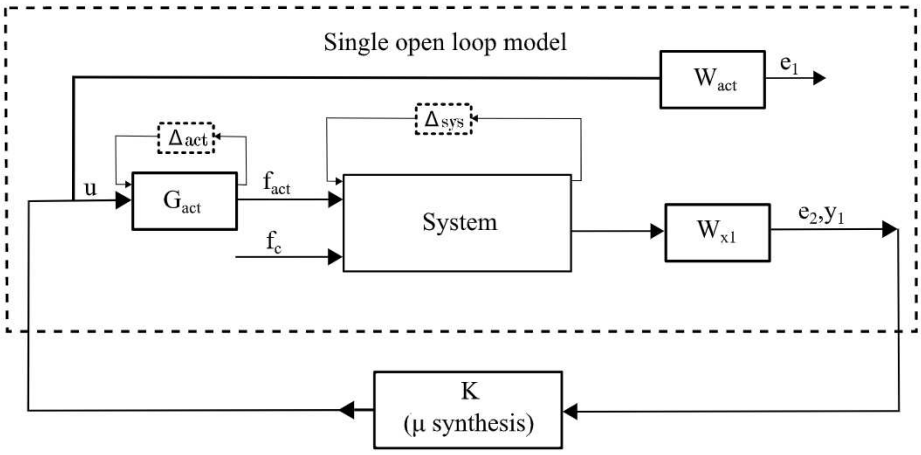

Fig. 7. μ synthesis control method.

4. Chatter stability modelling

Although the above-mentioned control strategies have been previously considered for active vibration control of chatter, this prior work has not considered the robotically assisted approach described in Section 2. This issue is critical because the structural dynamics of the robot, and the potential for loss-of-contact at the robot–workpiece interface, need to be considered. Consequently, the present study will benchmark all of these control strategies within this context. To do so, two models of machining chatter will be used.

The first approach is an analytical frequency domain prediction of chatter. This has the advantage of fast computation, however the approach assumes linear system behaviour which can reduce the accuracy of the results. The second approach is time domain modelling, which allows more complex nonlinear models of the mechanics, enabling more accurate results when actuator saturation occurs. However, the computational cost is higher and less theoretical insight can be obtained with this approach.

In the present study the stability was predicted using Budak and Altintas's method [5]. Details of this approach are outside the context of the current contribution, but the theory and method is widely reported elsewhere [5,6].

For time-domain modelling, a Simulink model [54] for simulating robotically assisted milling is used. The computations are carried out using a combination of Simulink [55] and a *c*-program that computes the milling kinematics. A feedback control method is applied to suppress the vibration on the workpiece. The workpiece is modelled with two degrees of freedom which are in the x and y directions. Only one direction is controlled and modelled in the present study. This direction is perpendicular to the feed direction as illustrated in Fig. 3. The chip thickness, forces and vibrations in two directions and the actuator force can be calculated by using the model. The system dynamics are modelled as transfer functions that represent the behaviour of the workpiece. Displacements along with the feed rate are used to update the relative position of the tool and workpiece.

The main advantage of the time-domain approach is that actuator saturation effects can be considered when evaluating the different vibration control strategies. Based upon the performance of the chosen actuator, the actuator force is limited at 27 N in the present study. The disadvantages of the time-domain approach are that the model is more computationally intensive, the boundary of chatter stability cannot be immediately determined, multiple simulations are required to assess this stability limit, and a suitable criteria is required to identify the stability boundary. This stability boundary was determined based upon the nondimensional chip thickness criterion [56]. Here, a non-dimensional chatter coefficient, η, is defined as:

$$\eta = \frac{h_{d,max}}{h_{s,max}} \tag{16}$$

where $h_{d,max}$ is the maximum chip thickness during dynamic time domain simulation, and $h_{s,max}$ is the desired chip thickness. The threshold of chatter is set at 1.06 as recommended in [56].

4.1. Machining scenario and controller tuning

In order to investigate the performance of the active vibration control approach, chatter stability analysis and simulations are performed using representative parameters for the cutting conditions. These are summarised in Table 2.

Two problems emerge when tuning the controller gain(s) and evaluating the performance of the different control strategies. Taking direct velocity feedback as an example, the performance is theoretically improved by simply increasing the controller gain. In practice, the first problem is that this can lead to nonlinear and suboptimal performance due to actuator saturation effects, reducing the effectiveness of the controller at avoiding chatter. The second problem is that unmodelled modes of vibration, or unmodelled actuator dynamics, can lead to control instability, as it is widely recognised in the active vibration control literature.

Table 2
Structural, machining and simulation parameters.

Preloaded structural parameters		Machining parameters	
Natural frequency	142.1 Hz	Tool diameter	16 mm
Damping ratio	0.88%	Number of teeth	4
Stiffness	2.43×10^7 N m^{-1}	Tool helix angle	30°
Flexible robot parameters		Material	Al-7075-T6
Natural frequency	23 Hz, 47 Hz	Cutting stiffness K_r	205×10^6 N m^{-2}
Damping ratio	4.3%, 2.9%	Cutting stiffness K_t	768×10^6 N m^{-2}
Stiffness	7.9×10^5 N m^{-1}, 2×10^6 N m^{-1}	Milling type	Down milling
Time domain simulation parameters		Radial depth of cut	Half immersion
Iteration per revolution	512	Feed per tooth	0.05 mm
Number of tool cycle	50		
Sample per iteration	8		
Axial tool layers	30		

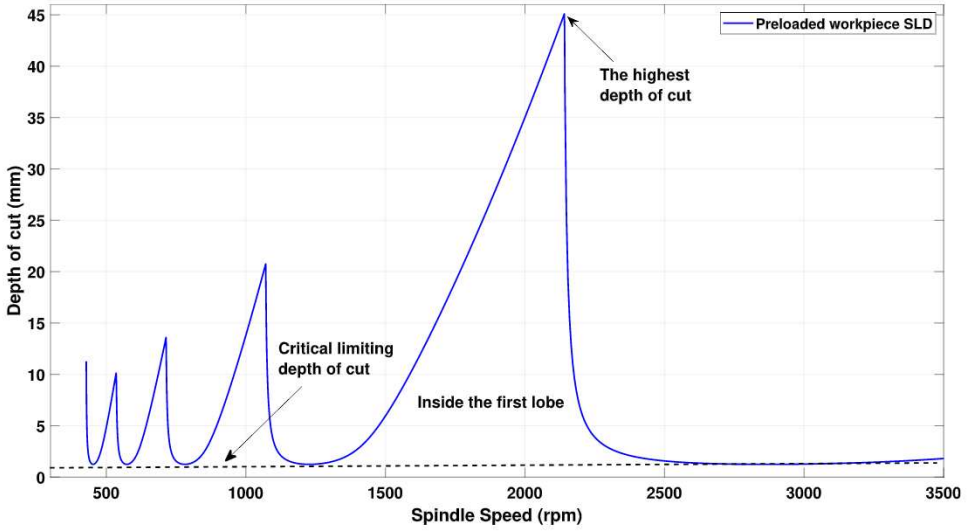

Fig. 8. Uncontrolled, preloaded workpiece SLD.

In the present study, the first problem is addressed by using a structured approach to controller tuning, in order to fairly compare all of the controllers (in simulations) whilst accounting for saturation affects. Following this, the second problem is addressed by performing experimental structural dynamics testing to evaluate the performance of the control systems.

4.1.1. Tuning approach

The tuning approach begins by considering the stability lobe diagram for the uncontrolled structure, as shown in Fig. 8. Here, the stability boundary is plotted as a function of spindle speed and axial depth of cut. It can be seen that the *critical limiting depth of cut* is approximately 1 mm: below this, no chatter can occur. This stability limit applies, for example, when the spindle speed is 2700 rpm. Meanwhile, the so-called *lobes* lead to regions of higher stability, one of which occurs near 2100 rpm that is the peak spindle speed of SLD. However, at 2100 rpm the forced vibrations are much higher since the excitation frequency is close to the natural frequency of the uncontrolled structure.

Two tuning scenarios are considered, and these are referred to as the maximum depth of cut (b_{max}) tuning and the critical limiting depth of cut (b_{crit}) tuning. In b_{max} tuning, the objective is to maximise the depth of cut $b = b_{max}$ at the peak spindle speed without causing instability, whilst simultaneously ensuring there is no actuator saturation. The peak spindle speed is defined as the spindle speed corresponding to the highest depth of cut, as illustrated on Fig. 8. It should be noted that the peak spindle speed can be shifted slightly as the controller gains are adjusted. From a practical perspective, this enables the maximal material removal rate by harnessing the 'lobe' effect observed in the stability lobe diagram.

In b_{crit} tuning, the objective is to maximise the critical limiting depth of cut, $b = b_{crit}$. However, the constraint is to ensure no saturation at $b = b_{crit}$, at the peak spindle speed. From a practical perspective, this enables maximal material rate regardless of the chosen spindle speed. The saturation constraint is still applied at the peak spindle speed because this condition is more likely to exhibit significant forced vibrations and is therefore considered to be a 'worst case' scenario for the onset of saturation.

Table 3
Tuning parameters.

Control method	Tuning parameters
Direct Velocity Feedback (DVF)	g_{dvf}
Virtual Passive Absorber (VPA)	μ_c
Proportional Integrated Derivative (PID)	g_a, g_v, g_p
Linear Quadratic Regulator (LQR)	Q, R
H Infinity (H_∞)	G_{st}, f_1, f_2
μ Synthesis	G_{st}, f_1, f_2

Table 4
Control effect on critical limiting and maximum depth of cut.

Control method	b_{crit} (mm)		b_{max} (mm)	
Base structure	0.8		27.2	
Uncontrolled	1.2		45.1	
	b_{crit} tuning		b_{max} tuning	
	b_{crit} (mm)	b_{max} (mm)	b_{crit} (mm)	b_{max} (mm)
DVF	3.2	47.2	2.3	46.6
VPA	2.5	46.5	1.8	46.3
PID	3.2	47.3	2.3	46.6
LQR	3.2	47.2	2.3	46.6
H_∞	3.1	46.2	2.6	46.3
μ synthesis	3.1	46.7	2.6	46.7

As mentioned previously the SADE algorithm is used to perform this numerical optimisation. SADE is a population based global optimisation algorithm where the fitness of each candidate solution is evaluated. The optimisation problem is implemented as follows, for the two respective scenarios:

For each candidate, the input to the optimisation problem is the set of controller gains, as summarised in Table 3. For example, only the scalar value g_{dvf} is tuned for the direct velocity feedback scenario. The frequency domain analysis is first used to determine the peak spindle speed and b_{max} (or b_{crit}). A time domain simulation is then run at the peak spindle speed. If saturation is observed (defined as an actuation force exceeding 27 N) then this candidate solution is assigned a fitness of zero. If not, the fitness is assigned a value equal to b_{max} (or b_{crit}). Consequently, the iterative optimisation algorithm will seek the controller gains which provide the maximum value of b_{max} (or b_{crit}) without inducing actuator saturation.

Once this tuning step is completed, the full stability of the controlled system is simulated for all spindle speeds. The time-domain approach is used to fully consider any actuator saturation effects, which might still arise at spindle speeds different to that used for the tuning process. Spindle speeds from 500 to 3000 rpm are explored at 100 rpm intervals, while the depth of cut is chosen with 0.1 mm intervals. In addition to identifying the onset of chatter stability, the simulations are used to determine the onset of actuator saturation effects. At each spindle speed, the depth of cut where actuator saturation first occurred was recorded. Actuator saturation was considered to occur when the actuator force exceeded 27 N.

5. Simulated results for chatter stability

Chatter stability predictions for the b_{crit} tuning scenario are shown in Fig. 9. In this scenario, the control objective is to maximise the limiting critical depth of cut, which can be considered as the 'least stable' machining scenario that is independent of the spindle speed. It can be seen that all the controllers achieve a substantial increase in this stability boundary. However, the time domain simulations indicate that all of the control strategies suffer from actuator saturation effects within the area that would normally have been a stable 'lobe' region near 2100 rpm. A possible consequence of this saturation is that the maximum stable depth of cut is reduced, as the controller becomes unable to deliver the necessary force to the structure.

The predicted stability boundaries for b_{max} tuning are shown in Fig. 10. In this scenario, the aim is to maximise the high possible stable depth of cut whilst also avoiding actuator saturation. It can be seen that all of the controllers perform similarly and that there are only small improvements in the maximum stable depth of cut. However, at other spindle speeds the relative improvement in stability is better, for example at 3000 rpm the limiting critical depth of cut is increased from 1.3 mm to 2.7 mm. This illustrates how actuator saturation effects can become very significant when considering the design of active vibration control regimes for chatter avoidance.

To summarise these results, the comparison of critical limiting and maximum depth of cut are given in Table 4, and the corresponding tuning parameters are listed in Table 5. With reference to Table 4, two benchmark comparisons are provided. The 'base structure' benchmark gives an indication of the stability of the original workpiece and flexure (as denoted in Fig. 3). The 'Uncontrolled' benchmark gives an indication of the stability when the beam and robot interface are considered, even with no control force applied to the proof-mass actuator. This latter scenario is the benchmark that was presented in Figs. 9 and 10.

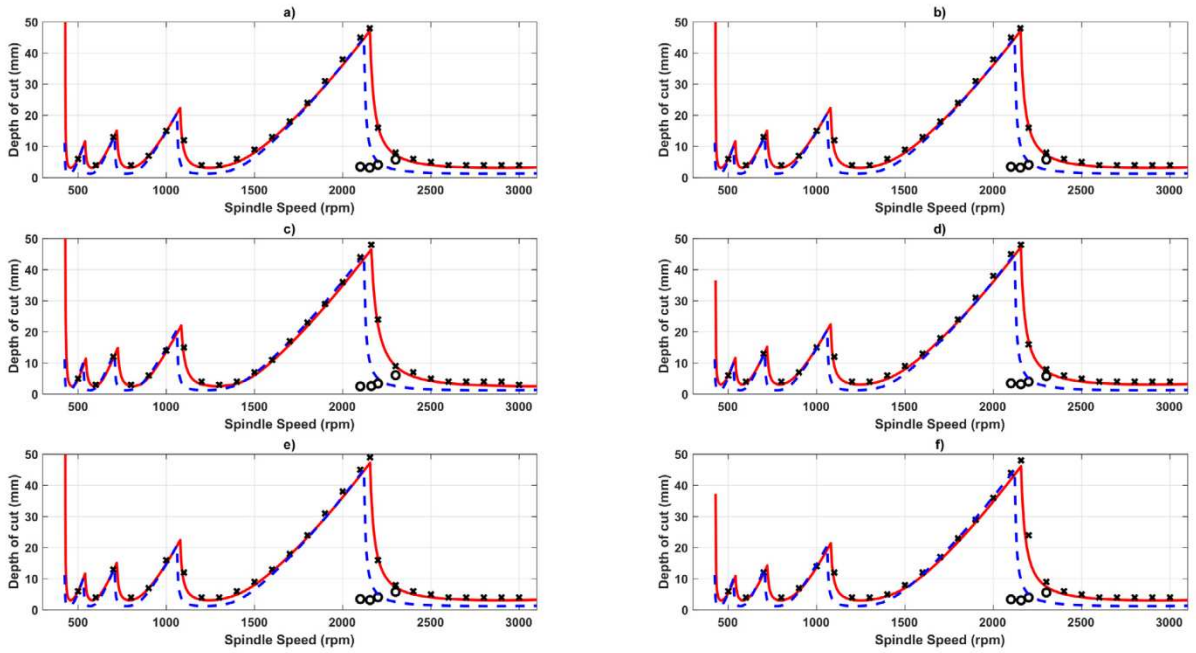

Fig. 9. Stability lobe diagrams for b_{crit} tuning. Red solid (——) lines show the controlled case and blue dashed (- - -) lines show the uncontrolled case, using the frequency domain chatter prediction. Circles (○) show the onset of saturation in the controlled case, and cross (×) symbols show the onset of chatter in the controlled case, using the time domain simulation. (a) Direct Velocity Feedback, (b) Virtual Passive Absorber, (c) PID control, (d) LQR control, (e) H_∞ control, (f) μ-synthesis control.

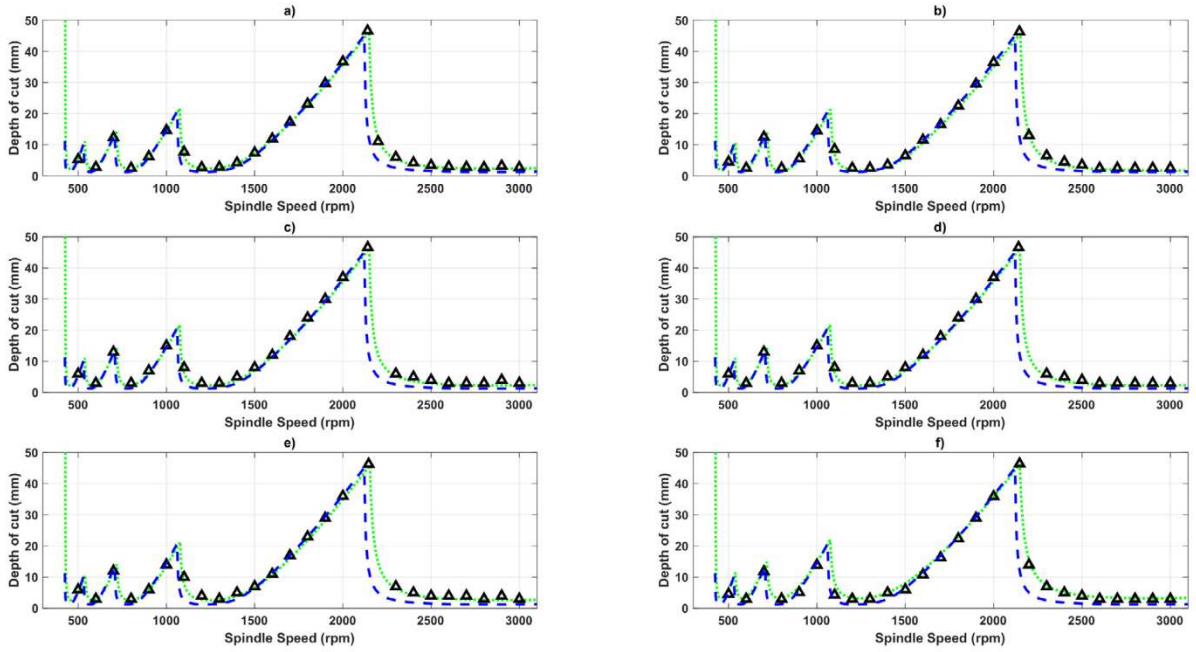

Fig. 10. Stability lobe diagrams for b_{max} tuning. Green dotted (·····) lines show the controlled case and blue dashed (- - -) lines show the uncontrolled case, using the frequency domain chatter prediction. Triangle (Δ) symbols show the onset of chatter in the controlled case, using the time domain simulation. No actuator saturation usually occurs for this scenario, owing to the controller tuning methodology. (a) Direct Velocity Feedback, (b) Virtual Passive Absorber, (c) PID control, (d) LQR control, (e) H_∞ control, (f) μ-synthesis control.

Table 5
Control parameters for the critical limiting and maximum depth of cut.

Control method	b_{crit} tuning	b_{max} tuning
DVF	g = 235	g = 135
VPA	$\mu = 0.002,\ \zeta = 0.027$	$\mu = 0.0004,\ \zeta = 0.013$
PID	$g_{pa} = 1\times10^{-6},\ g_{pv} = 236,\ g_{pp} = 1\times10^{4}$	$g_{pa} = 7.52\times10^{-5},\ g_{pv} = 129,\ g_{pp} = 4.25\times10^{3}$
LQR	$Q_1 = 6793.3,\ R = 0.024$	$Q_1 = 9219.8,\ R = 0.065$
H_∞	$G_{st} = 4.7\times10^{5},\ f_1 = 252.7,\ f_2 = 55.8$	$G_{st} = 5.3\times10^{5},\ f_1 = 462.8,\ f_2 = 40.6$
μ synthesis	$G_{st} = 1.9\times10^{7},\ f_1 = 2659,\ f_2 = 4.37$	$G_{st} = 1.7\times10^{7},\ f_1 = 3035.04,\ f_2 = 3.02$

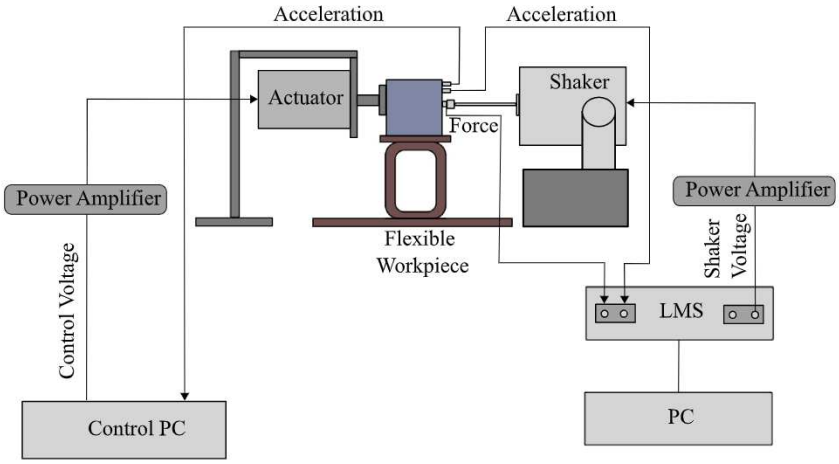

Fig. 11. Test setup for the experimental FRF measurement.

6. Experimental validation — frequency response function testing

To validate the simulated FRF results, several experiments are performed using a test setup shown in Fig. 11. The flexible workpiece is clamped to the base and an electromagnetic shaker is used to excite the workpiece by a harmonic chirp signal. The actuator and flexible arm are adjusted so that they exert a preload force against the workpiece. A force sensor and an accelerometer are mounted to measure the frequency response of the workpiece, and its response is processed using LMS software. To suppress the vibration, the acceleration of the workpiece is measured and converted to velocity/displacement to apply each control method using Simulink software. A multi-channel IO-card (NI PCIe-6321) is used for the feedback control system, using a sampling period of 50 μs. A control voltage is sent from the control PC in real-time to drive the actuator once the acceleration of the workpiece is processed by the controller.

The resulting performance is compared to the theoretical predictions in Fig. 12.

All the experimental FRF results match well with the simulated FRF results, although some additional modes of vibration are observed in the experimental data at higher frequencies. These could be associated with unmodelled modes of vibration or actuator dynamics.

7. Discussion

Some aspects of the results merit further discussion. First, there are some nuances of μ-synthesis control worth considering, particularly regarding uncertainties. In the present study, 20% dynamic (frequency-dependent) uncertainty (Δ_{act}) was added to the actuator around the natural frequency of the flexible workpiece. Meanwhile, 20% parametric (real) uncertainty (Δ_{sys}) was added to the modal parameters of the structure. The resulting optimised control parameters were given in Table 5. The bode diagram for the nominal system, with only actuator uncertainty and with the all uncertainties is shown in Fig. 13. Since the uncertainties are the dynamic and parametric uncertainties, $D, G-K$ iteration procedure was used to find the optimum μ value. The controller can tolerate $1/\mu$ times more uncertainty and yields the performance target. The same controller gains chosen for H_∞ control can be used adjusting the uncertainty percentages until the μ value gets close to 1. Instead of using the same gains, the controller gains are optimised using SADE algorithm in order to keep the uncertainties fixed as suggested in the literature [43].

To implement the proposed method in practice would require a serial arm robot instead of the simplified flexible structure depicted in Fig. 3(a). This robot could exhibit additional modes of vibration in addition to those that were considered in the model and design process. Consequently, further frequency response function testing would be needed to ensure that these modes of vibration did not destabilise the active controller.

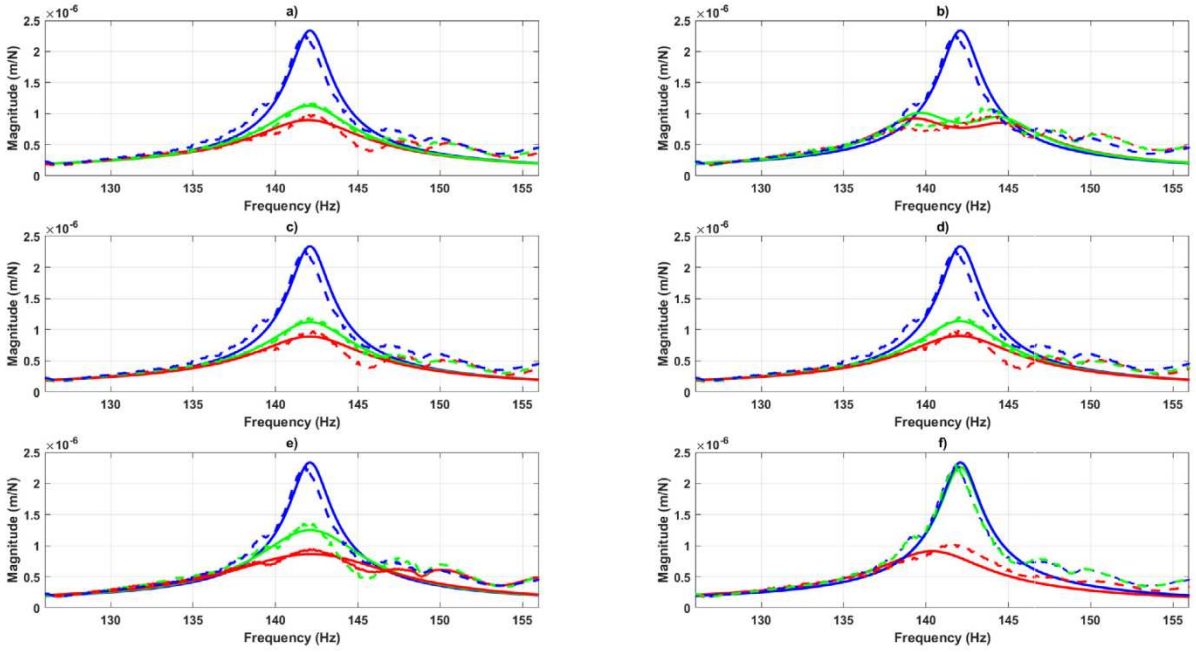

Fig. 12. Simulated and experimental FRF results. Red (——) lines show the b_{crit} tuning, green (——) lines show the b_{max} tuning, and blue (——) lines show the uncontrolled case. Solid lines show the theoretical predictions while the dashed lines show the experimental FRFs. (a) Direct Velocity Feedback, (b) Virtual Passive Absorber, (c) PID control, (d) LQR control, (e) H_∞ control, (f) μ-synthesis control.

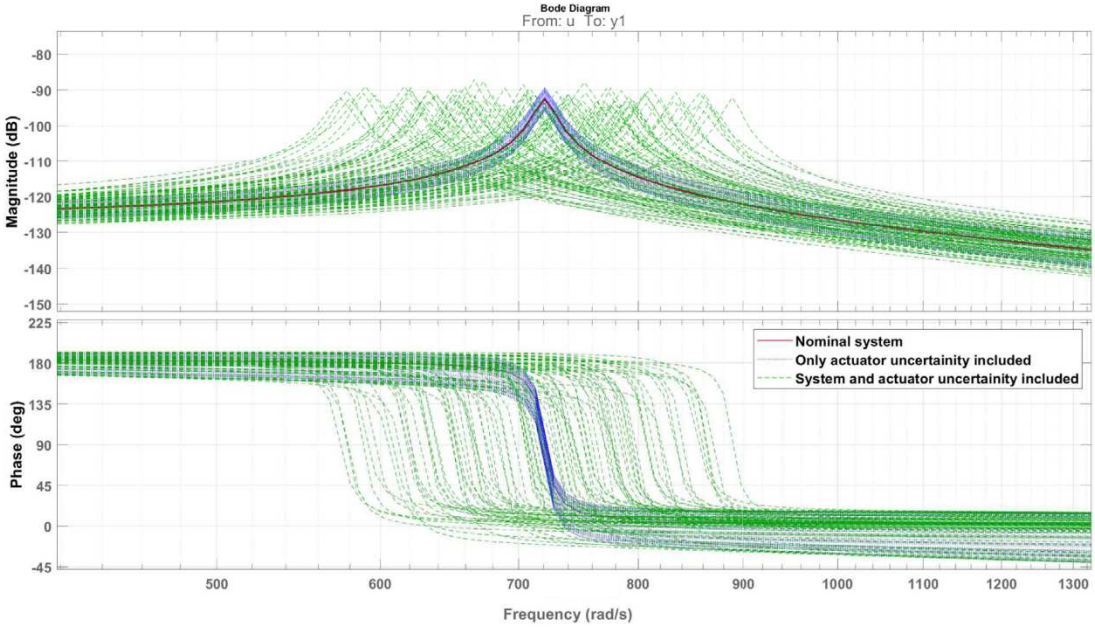

Fig. 13. The model with uncertainties. Nominal system (——), only actuator uncertainty included (------), system and actuator uncertainty included (– – –).

However, the real robot would then be able to reposition the contact point between its end effector (including the proof mass actuator) and the workpiece. This would enable new possibilities for adaptive control of the workpiece as the machining operations progress along the workpiece surface. As material is removed from the workpiece, controller re-tuning may also be required. Furthermore, the contact location of the tool on the workpiece will also change as material is removed. This could be an aspect where μ synthesis control becomes more beneficial, to cope with the associated uncertainties.

In the present study, Altintas and Budak's zero-order approach is chosen for predicting chatter stability boundaries as it is a widely accepted, fast, and accurate method. Even though the same chatter boundaries are obtained by other chatter models such as homotopy, Chebyshev polynomials [2], semi or full-discretisation methods [32], they could be used to predict the chatter boundaries. Nonetheless, choosing a different prediction method would result in longer computation time for chatter boundary prediction and optimisation of the controller parameters.

A risk with the proposed method is that loss of contact may occur between the robot end effector and the workpiece itself. This can be avoided by adjusting the robot position to ensure a static pre-load force that exceeds the amplitude of the dynamic forces generated by the proof mass actuator. However, in practical machining scenarios the forced vibrations from the machining process could also induce loss-of-contact. This would cause nonlinear behaviour and degrade the performance of the active control system.

The actuator bandwidth is another aspect to consider. If the workpiece and chatter frequencies exceed the bandwidth of the actuator then the chatter stability will obviously not be improved. However, in these scenarios the onset of chatter is less likely due to the process damping phenomenon [57].

Finally, with the proposed method the system design could choose different types of contact between the robot end effector and the workpiece. In the present study a rigid metallic contact was chosen. However, alternative contact configurations could be used, potentially including a rolling contact to enable continuous motion of the end effector during machining. Such changes would also impact on the controllability of the system, as they would change the transmission of force between the proof mass actuator and the workpiece.

8. Conclusion

A novel configuration of robotically assisted milling has been proposed that seeks to improve the chatter stability by using active vibration control. The feasibility of this approach has been assessed using a simplified scenario, and the main conclusions that can be drawn are:

- The limiting critical depth of cut (b_{crit}) can be increased by a factor of 2.6, compared to a system with no vibration control, and by a factor of 4 compared to a system with no robotic assistance/additional support.
- Many standard control methods (DVF, VPA, PID, LQG, H_∞ and μ synthesis) are effective in achieving this performance improvement, and that there is no significant difference in performance between the different control strategies.
- The practical performance is limited by actuator saturation effects, owing to the high amplitudes of forced vibration that occur during milling. This actuator saturation needs to be carefully considered when tuning the control system gains. As a result of the actuator saturation, the maximum possible depth of cut (b_{max}) was not substantially improved even though the limiting critical depth of cut (b_{crit}) was increased considerably by a factor of 2.6.
- In the present study, controller tuning was achieved using numerical optimisation methods, combined with analytical and time-domain predictions of the system performance. In future work, alternative methods for tuning could be explored in order to avoid actuator saturation from a theoretical basis.

To conclude, the proposed approach has been shown to be a feasible method for improving the stability of milling based upon robotically assisted milling concepts. Further work is needed to demonstrate this in practice.

Declaration of competing interest

The authors declare that they have no known competing financial interests or personal relationships that could have appeared to influence the work reported in this paper.

Acknowledgement

The first author would like to acknowledge the support from the Turkish Ministry of National Education by providing the scholarship.

References

[1] G. Quintana, J. Ciurana, Chatter in machining processes: A review, Int. J. Mach. Tools Manuf. 51 (5) (2011) 363–376.
[2] D. Olvera, A. Elías-Zúñiga, H. Martínez-Alfaro, L.L. De Lacalle, C. Rodríguez, F. Campa, Determination of the stability lobes in milling operations based on homotopy and simulated annealing techniques, Mechatronics 24 (3) (2014) 177–185.
[3] U. Bravo, O. Altuzarra, L.L. De Lacalle, J. Sánchez, F. Campa, Stability limits of milling considering the flexibility of the workpiece and the machine, Int. J. Mach. Tools Manuf. 45 (15) (2005) 1669–1680.
[4] F. Campa, L.L. De Lacalle, A. Celaya, Chatter avoidance in the milling of thin floors with bull-nose end mills: Model and stability diagrams, Int. J. Mach. Tools Manuf. 51 (1) (2011) 43–53.
[5] Y. Altintaş, E. Budak, Analytical prediction of stability lobes in milling, CIRP Ann.-Manuf. Technol. 44 (1) (1995) 357–362.
[6] Y. Altintas, Manufacturing Automation: Metal Cutting Mechanics, Machine Tool Vibrations, and CNC Design, Cambridge University Press, 2012.
[7] G. Urbikain Pelayo, L. López De La Calle, Stability charts with large curve-flute end-mills for thin-walled workpieces, Mach. Sci. Technol. 22 (4) (2018) 585–603.
[8] F.I. Compean, D. Olvera, F. Campa, L.L. De Lacalle, A. Elias-Zuniga, C. Rodriguez, Characterization and stability analysis of a multivariable milling tool by the enhanced multistage homotopy perturbation method, Int. J. Mach. Tools Manuf. 57 (2012) 27–33.

[9] D. Olvera, A. Elías-Zúñiga, O. Martínez-Romero, L. López de Lacalle, H. Martínez-Alfaro, H. Siller, M. Pineda, Improved predictions of the stability lobes for milling cutting operations of thin-wall components by considering ultra-miniature accelerometer mass effects, Int. J. Adv. Manuf. Technol. 86 (5) (2016) 2139–2146.
[10] J. Den Hartog, Mechanical Vibrations, Vol. 122, McGraw, Hill, 1934.
[11] N.D. Sims, Vibration absorbers for chatter suppression: a new analytical tuning methodology, J. Sound Vib. 301 (3–5) (2007) 592–607.
[12] S. Tobias, Machine Tool Vibration, Blackie, London, 1965.
[13] J. Munoa, I. Mancisidor, N. Loix, L. Uriarte, R. Barcena, M. Zatarain, Chatter suppression in ram type travelling column milling machines using a biaxial inertial actuator, CIRP Ann.-Manuf. Technol. 62 (1) (2013) 407–410.
[14] J. Munoa, X. Beudaert, K. Erkorkmaz, A. Iglesias, A. Barrios, M. Zatarain, Active suppression of structural chatter vibrations using machine drives and accelerometers, CIRP Ann. 64 (1) (2015) 385–388.
[15] A. Bilbao-Guillerna, A. Barrios, I. Mancisidor, N. Loix, J. Munoa, Control laws for chatter suppression in milling using an inertial actuator, in: Proceedings of ISMA 2010-International Conference on Noise and Vibration Engineering, 2010, pp. 1–12.
[16] I. Mancisidor, J. Munoa, R. Barcena, Optimal control laws for chatter suppression using inertial actuator in milling processes, in: 11th International Conference on High Speed Machining (HSM2014), 2014.
[17] M. Law, M. Wabner, U. Frieß, S. Ihlenfeldt, Improving machining performance of in-use machine tools with active damping devices, in: 3rd International Chemnitz Manufacturing Colloquium ICMC, 2014, pp. 393–412.
[18] R. Kleinwort, M. Schweizer, M.F. Zaeh, Comparison of different control strategies for active damping of heavy duty milling operations, Proc. Cirp 46 (2016) 396–399.
[19] M. Zaeh, R. Kleinwort, P. Fagerer, Y. Altintas, Automatic tuning of active vibration control systems using inertial actuators, CIRP Ann. 66 (1) (2017) 365–368.
[20] N. Esfandi, Stability and Control for Machining of Thin-Walled Structures-A Time-Varying Delayed Distributed Parameter System (Ph.D. thesis), UCLA, 2017.
[21] N. van Dijk, N. van de Wouw, E. Doppenberg, H. Oosterling, H. Nijmeijer, Chatter control in the high-speed milling process using μ-synthesis, in: Proceedings of the 2010 American Control Conference, IEEE, 2010, pp. 6121–6126.
[22] N.J. van Dijk, N. van de Wouw, E.J. Doppenberg, H.A. Oosterling, H. Nijmeijer, Robust active chatter control in the high-speed milling process, IEEE Trans. Control Syst. Technol. 20 (4) (2011) 901–917.
[23] N. Van de Wouw, N. van Dijk, A. Schiffler, H. Nijmeijer, E. Abele, Experimental validation of robust chatter control for high-speed milling processes, in: Time Delay Systems, Springer, 2017, pp. 315–331.
[24] A. Verl, A. Valente, S. Melkote, C. Brecher, E. Ozturk, L.T. Tunc, Robots in machining, CIRP Ann. 68 (2) (2019) 799–822.
[25] A. Barrios, S. Mata, A. Fernandez, J. Munoa, C. Sun, E. Ozturk, Frequency response prediction for robot assisted machining, MM Sci. J. 2019 (04) (2019) 3099–3106.
[26] C. Sun, P.L. Kengne, A. Barrios, S. Mata, E. Ozturk, Form error prediction in robotic assisted milling, in: Procedia CIRP, Vol. 82, Elsevier, 2019, pp. 491–496.
[27] N. Esfandi, T.-C. Tsao, Robot assisted machining of thin-walled structures, IFAC-PapersOnLine 50 (1) (2017) 14594–14599.
[28] E. Ozturk, A. Barrios, C. Sun, S. Rajabi, J. Munoa, Robotic assisted milling for increased productivity, CIRP Ann. (2018).
[29] Operational, M. Manual, Micromega Dynamics, Belgium, 2019.
[30] A. Preumont, Vibration Control of Active Structures, Vol. 2, Springer, 1997.
[31] M. Ozsoy, N. Sims, E. Ozturk, Investigation of an actively controlled robot arm for vibration suppression in milling, in: EURODYN 2020: Proceedings of the XI International Conference on Structural Dynamics, European Association for Structural Dynamics (EASD), 2020, pp. 4577–4589.
[32] J. Munoa, X. Beudaert, Z. Dombovari, Y. Altintas, E. Budak, C. Brecher, G. Stepan, Chatter suppression techniques in metal cutting, CIRP Ann. 65 (2) (2016) 785–808.
[33] S. Huyanan, N.D. Sims, Vibration control strategies for proof-mass actuators, J. Vib. Control 13 (12) (2007) 1785–1806.
[34] K. Worden, G. Manson, On the identification of hysteretic systems. Part I: Fitness landscapes and evolutionary identification, Mech. Syst. Signal Process. 29 (2012) 201–212.
[35] I. Mancisidor, J. Munoa, R. Barcena, X. Beudaert, M. Zatarain, Coupled model for simulating active inertial actuators in milling processes, Int. J. Adv. Manuf. Technol. 77 (1–4) (2015) 581–595.
[36] A. Bilbao-Guillerna, I. Azpeitia, S. Luyckx, N. Loix, J. Munoa, Low frequency chatter suppression using an inertial actuator, 2012.
[37] Y. Tarng, J. Kao, E. Lee, Chatter suppression in turning operations with a tuned vibration absorber, J. Mater Process. Technol. 105 (1–2) (2000) 55–60.
[38] E.I. Rivin, H. Kang, Enhancement of dynamic stability of cantilever tooling structures, Int. J. Mach. Tools Manuf. 32 (4) (1992) 539–561.
[39] H.O. Bansal, R. Sharma, P. Shreeraman, Pid controller tuning techniques: a review, J. Control Eng. Technol. 2 (4) (2012) 168–176.
[40] S. Paul, R. Morales-Menendez, Active control of chatter in milling process using intelligent PD/PID control, IEEE Access 6 (2018) 72698–72713.
[41] C.-H. Yeung, Y. Altintas, K. Erkorkmaz, Virtual CNC system. Part i. system architecture, Int. J. Mach. Tools Manuf. 46 (10) (2006) 1107–1123.
[42] M. Fallah, B. Moetakef-Imani, Design, analysis, and implementation of a new adaptive chatter control system in internal turning, Int. J. Adv. Manuf. Technol. 104 (5–8) (2019) 1637–1659.
[43] S. Skogestad, I. Postlethwaite, Multivariable Feedback Control: Analysis and Design, Vol. 2, Wiley New York, 2007.
[44] Y. He, X. Chen, Z. Liu, Y. Chen, Active vibration control of motorized spindle based on mixed H/Kalman filter robust state feedback control, J. Vib. Control (2019) 1077546318820935.
[45] F. Shi, H. Cao, X. Zhang, X. Chen, A chatter mitigation technique in milling based on h∞-ADDPMS and piezoelectric stack actuators, Int. J. Adv. Manuf. Technol. 101 (9–12) (2019) 2233–2248.
[46] F. Chen, Active Damping of Machine Tools with Magnetic Actuators (Ph.D. thesis), University of British Columbia, 2014.
[47] G.S. Duncan, M.H. Kurdi, T.L. Schmitz, J.P. Snyder, Uncertainty propagation for selected analytical milling stability limit analyses.
[48] D. Hajdu, T. Insperger, D. Bachrathy, G. Stepan, Prediction of robust stability boundaries for milling operations with extended multi-frequency solution and structured singular values, J. Manuf. Process. 30 (2017) 281–289.
[49] D. Hajdu, T. Insperger, G. Stepan, Robust stability analysis of machining operations, Int. J. Adv. Manuf. Technol. 88 (1–4) (2017) 45–54.
[50] J.C. Doyle, Synthesis of robust controllers and filters, in: The 22nd IEEE Conference on Decision and Control, IEEE, 1983, pp. 109–114.
[51] A. Packard, J. Doyle, The complex structured singular value, Automatica 29 (1) (1993) 71–109.
[52] P.M. Young, Controller design with mixed uncertainties, in: Proceedings of 1994 American Control Conference-ACC'94, Vol. 2, IEEE, 1994, pp. 2333–2337.
[53] P.M. Wortelboer, O.H. Bosgra, Generalized frequency weighted balanced reduction, in: [1992] Proceedings of the 31st IEEE Conference on Decision and Control, IEEE, 1992, pp. 2848–2849.
[54] N.D. Sims, The self-excitation damping ratio: a chatter criterion for time-domain milling simulations, 2005.
[55] MATLAB, 9.7.0.1190202 (R2019b), The MathWorks Inc., Natick, Massachusetts, 2018.
[56] M.L. Campomanes, Y. Altintas, An improved time domain simulation for dynamic milling at small radial immersions, J. Manuf. Sci. Eng. 125 (3) (2003) 416–422.
[57] Y. Altintas, M. Weck, Chatter stability of metal cutting and grinding, CIRP Ann. 53 (2) (2004) 619–642.